Hydraulic and Mechanical Behavior of Unsaturated Silt: Experimental and Theoretical Characterization

Tiantian Ma, Ph.D.[1]; Changfu Wei[2]; Houzhen Wei, Ph.D.[3]; and Wentao Li, Ph.D.[4]

Abstract: A series of experiments were performed to investigate the hydraulic and mechanical behavior of an unsaturated silt obtained from the Yellow River Delta. To identify the key factors that influence the soil-water characteristics (SWC), an experimental program was designed to study the SWC of the soil at different void ratios and vertical pressures. It was shown that an apparent hysteresis phenomenon occurred on the SWC curves when the soil experienced drying/wetting cycles. It was also shown that the influence of void ratio on the SWC was significant, and the stress state influenced the SWC only through changing the void ratio. Isotropic compression tests were conducted at different constant matric suctions, using a suction-controlled *double cell* triaxial apparatus. The soil under shearing showed apparent dilatant and softening behavior, in a way similar to medium to dense sand. In addition, the hardening effect of matric suction was significant, and both the stiffness and peak strength of the soil increased with matric suction. Based on the experimental observations, an elastoplastic constitutive model coupling capillary hysteresis and plastic deformation was developed, in which a hysteretic SWC relationship was introduced to characterize the influence of hydraulic history on the skeletal deformation. To better simulate the volumetric change of the soil, a nonassociated flow rule was adopted. The effect of the plastic volumetric strain on water-retention behavior was also taken into consideration. The proposed model was used to simulate the behavior of unsaturated silt under constant-suction, isotropic compression and constant-suction, triaxial shearing conditions, showing the capability of the new model in describing the behavior of unsaturated silt. **DOI: 10.1061/(ASCE)GM.1943-5622.0000576.**

Author keywords: Unsaturated soil; Compacted silt; Dilatancy; Soil-water characteristic curve; Triaxial test; Elastoplastic constitutive model.

Introduction

Many types of unsaturated soils, including clay, silt, and sand, show apparent dilatant behavior under shearing conditions. Traditionally, research efforts (either experimental or theoretical) were mainly devoted to investigating the hydraulic and mechanical behavior of unsaturated soils without showing dilatant behavior. Although a few experimental studies have been performed on the behavior of nondilatant unsaturated clay (Sun et al. 2007a, b; Boyd and Sivakumar 2011; Toll 1990; Wheeler and Sivakumar 1995; Maatouk et al. 1995), the dilatant behavior of unsaturated soils remains largely unexplored. Perhaps the reason for this is due to the fact that, in unsaturated soil experiments, it is generally difficult to either control or measure the matric suction, and technical difficulties also exist in accurately measuring the volume change of unsaturated soils (Ng et al. 2002).

Several experimental studies on the dilatant behavior of unsaturated soils under shearing have been conducted (Cui and Delage 1996; Ng and Zhou 2005; Alonso et al. 2007). Cui and Delage (1996) performed a series of experiments on an unsaturated compacted silt in an osmotic suction–controlled triaxial apparatus and found that both stiffness and peak resistance of the soil increased with increasing suction, and the soil clearly showed dilatant behavior during shearing. To simulate the volumetric change of the soil during shearing, a hyperbolic formulation of a nonassociated flow rule was introduced (Cui and Delage 1996). Ng and Zhou (2005) performed direct shear tests on a compacted residual soil from granite under suction-controlled conditions and found that the maximum dilatancy depended strongly on matric suction and density. Alonso et al. (2007) presented experimental results on the dilatant behavior of a compacted coarse gravel of hard limestone by performing suction-controlled triaxial tests. They found that, to describe the behavior of coarse granular materials in the elastoplastic framework, the flow rule had to be defined in such a way that the suction dependency of plastic flow direction must be properly addressed. It is remarkable that the effect of the suction on dilatancy is opposite that of confining stress, and the dilatancy becomes more significant when the suction is higher.

In the past two decades, several constitutive models of unsaturated soils with coupling capillary effect and stress-strain behavior have been developed (Sun et al. 2007; Boyd and Sivakumar 2011; Toll 1990; Wheeler and Sivakumar 1995; Maatouk et al. 1995; Wheeler et al. 2003; Khalili et al. 2008; Gallipoli et al. 2003). Since the first integrated model of unsaturated soil (Alonso et al. 1990) appeared, numerous constitutive models of unsaturated soil have

[1]Assistant Professor, State Key Laboratory of Geomechanics and Geotechnical Engineering, Institute of Rock and Soil Mechanics, Chinese Academy of Sciences, Hubei 430071, China. E-mail: ttma@whrsm.ac.cn

[2]Professor, State Key Laboratory of Geomechanics and Geotechnical Engineering, Institute of Rock and Soil Mechanics, Chinese Academy of Sciences, Wuhan, Hubei 430071, China; College of Civil and Architectural Engineering, Guilin Univ. of Technology, Guilin, Guangxi 541004, China (corresponding author). E-mail: cfwei@whrsm.ac.cn

[3]Associate Professor, State Key Laboratory of Geomechanics and Geotechnical Engineering, Institute of Rock and Soil Mechanics, Chinese Academy of Sciences, Wuhan, Hubei 430071, China. E-mail: weihouzhen@163.com

[4]Doctoral Candidate, State Key Laboratory of Geomechanics and Geotechnical Engineering, Institute of Rock and Soil Mechanics, Chinese Academy of Sciences, Wuhan, Hubei 430071, China. E-mail: lwtdn@sina.com

Note. This manuscript was submitted on May 28, 2014; approved on June 29, 2015; published online on December 31, 2015. Discussion period open until May 31, 2016; separate discussions must be submitted for individual papers. This paper is part of the ***International Journal of Geomechanics***, © ASCE, ISSN 1532-3641.

been developed. Some typical models have been compared and evaluated, based on the benchmark results of suction-controlled and constant water content laboratory tests (D'onza et al. 2011). In recent years, many constitutive models for unsaturated soils have been proposed by incorporating the effect of capillary hysteresis (Wheeler et al. 2003; Gallipoli et al. 2003; Sun et al. 2007; Tamagnini 2004; Sheng et al. 2004).

As well recognized, the density and the stress history are the two key factors that control the dilatant behavior of the soils (Been and Jefferies 1985). To take into account the effect of the initial state of sand, Been and Jefferies (1985) introduced a state parameter into the stress-dilatancy relationship, which represents the difference of void ratios between the current state and the critical state. Manzari and Dafalias (1997) proposed a critical-state two-surface plasticity model for sands, in which the nonassociated flow rule was adopted. In this model, a relationship between the peak stress ratio, dilatancy stress ratio, critical stress ratio, and state parameter was developed. Based on the experimental results of sand, Li and Dafalias (2000) proposed a general expression for describing the dilatancy based on the micromechanical analysis. Later on, Chiu and Ng (2003) introduced this relationship into a constitutive model of unsaturated soils, in which the material parameters and critical state were assumed to depend upon the matric suction. Miller et al. (2008) presented experimental results that documented the effect of solid deformations on soil-water characteristic curves (SWCCs) of silts. The proposed elastoplastic phenomenological constitutive model based on the bounding surface plasticity theory was capable of predicting hysteresis in SWCCs and the coupled mechanical–hydraulic behavior of unsaturated soils. Liu and Muraleetharan (2012a, b) presented a comprehensive constitutive model for unsaturated sands and silts, in which the hysteresis SWCC model was introduced. With the incorporation of the bounding surface plasticity concept, the proposed model could simulate the unsaturated silt/sand behavior under either monotonic or cyclic loading conditions.

In the present work, a series of experiments were performed to investigate the hydraulic and mechanical behavior of an unsaturated compacted silt obtained from the Yellow River Delta. Based on the experimental observations, an elastoplastic constitutive model of unsaturated dilatant soils, which is capable of describing the coupling effect of capillary hysteresis and plastic deformation, is developed within the framework of critical-state soil mechanics. Although both the capillary hysteresis and skeletal plastic deformation as well as their coupling are of main concerns, special attention is paid to the dilatant and softening behavior of unsaturated soil under shearing conditions.

Experimental Materials

The tested material is a silty soil, sampled from the Yellow River Delta. The physical properties of the soil are given in Table 1, and the distribution curve of grain sizes is shown in Fig. 1. The result of the standard proctor compaction test shows that the maximum dry density of the soil is 1.70 g/cm^3 with an optimum water content of 19.4%.

The soil was first air dried and then carefully wetted with a prescribed amount of deionized water to reach a specified water content of approximately 16%. The soil was put in tightly covered plastic bags and stored in a container with both temperature and humidity being controlled for several days for moisture equilibration. The soil samples were statically compacted with an initial water content of 16%, layer by layer, in a cylindrical mold. All tests were carried out in temperature-controlled rooms at 20 ± 1°C.

Prior to conducting the research experiments, numerous tests were conducted to calibrate and evaluate the performance of the testing device [including the pressure plate extractor, one-dimensional (1D) stress-controlled pressure plate extractor, and the *double cell* triaxial GDS-HUKUST apparatus (GDS, Hampshire, U.K.)] with respect to experimental error and repeatability.

Soil-Water Characteristics

To explore the key factors that influence the soil-water characteristics (SWC), two types of tests were performed on (1) the samples with different initial void ratios and (2) the samples with different vertical stresses, respectively.

Effect of Initial Void Ratio

A conventional pressure plate extractor was used to determine the SWCCs of the silt with different void ratios. The matric suction was controlled using the axis translation method (Hilf 1956). All samples were prepared by static compaction in a mold with an inner diameter of 61.8 mm and a height of 20 mm. The dry densities of the samples varied from 1.35 to 1.70 g/cm^3, with void ratios varying from approximately 0.945 to 0.68. Before the test, the ceramic disks and the samples were carefully saturated. Then, the samples were carefully placed on the saturated ceramic disks, so that the samples had a good contact with the ceramics with minimum disturbance.

The SWCCs of the compacted silt with different initial void ratios are shown in Fig. 2. Clearly, as the void ratio decreases or the soil becomes denser, both the air-entry value and the residual degree of saturation increase, and thus the SWCC shifts rightward. This is

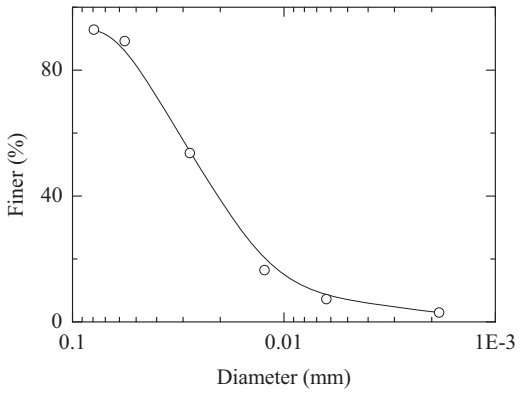

Fig. 1. Grading curve of the tested silt

Table 1. Index Properties of Silt

Specific gravity (G_s)	Liquid limit (ω_L, %)	Plastic limit (ω_P, %)	Plasticity index (I_P)	0.25~0.075 mm (%)[a]	0.075~0.005 mm (%)[a]	<0.005 mm (%)[a]
2.71	29.4	19.8	9.6	7.82	86.18	6.0

[a]Grain size.

an expected result, because a decrease in void ratio can block part of the passageways, resulting in an increase in the air-entry value (Ng and Pang 2000). From Fig. 2, it can be seen that the shape of SWCCs changes quite slightly with the void ratio.

Effect of Vertical Stress

Stress-dependent SWCC (SDSWCC) describes the relationship between suction and degree of saturation of a soil under a specified vertical stress.

1D-SDSWCC Experiments

In this study, a 1D stress-controlled pressure plate extractor (1D-SDSWCC) by GeoExpert (Embrach, Switzerland) was used to determine the drying and wetting boundaries of SWCCs under different vertical stresses. Compared with the traditional pressure plate extractor, this apparatus can apply 1D vertical stress (i.e., K_0 state), with the vertical displacement being accurately monitored.

The samples were compacted statically in a mold, with an inner diameter of 71 mm and a height of 19 mm. In the 1D SDSWCC experiments, all samples had an initial dry density of approximately $1.6\,\mathrm{g/cm^3}$ and an initial void ratio of 0.7.

The testing procedure is similar to that adopted in the traditional pressure plate extractor. After the sample was saturated and set up on the apparatus, the saturated sample was compressed under a specified vertical stress. After the compression was completed, the sample was dried by increasing the imposed matric suction step by step under the applied vertical stress. In the tests, SWCCs under four vertical stresses of 0, 100, 200, and 300 kPa were obtained. Under the four vertical stresses, the final axial displacements of the samples were 0, 0.2, 0.4, and 0.4 mm, respectively. Under the vertical stress of 100 kPa, the sample was wetted by decreasing the matric suction to 0 kPa after the drying stage.

Results and Discussion

Fig. 3 shows the water-retention curves under the four different vertical stresses. It can be seen that the SWCCs show clear hysteresis during a wetting-drying cycle. The SWCCs are nearly identical when the vertical stress varies from 0 to 300 kPa, implying that the effect of vertical stress on the SWCC is insignificant. This result can be easily understood, because the volumetric deformation of the soil matrix under the applied vertical stress is very small, and the void ratios of all samples are practically the same and remain unchanged during the compression process. By comparing with the experimental results at the different void ratios, one can conclude that the SWC does not depend directly upon the applied stress, and the stress state can influence the SWC only through the deformation of the soil matrix, i.e., the change in the void ratio and pore configuration. This result is consistent with the previous experimental data (Sun et al. 2007).

In addition, Fig. 3 reveals that, at $s_c = 0$ kPa during the wetting process, the degree of saturation is approximately 84%. That is, the soil did not reach the fully saturated condition during a wetting process. When the matric suction decreases to 0 kPa, a small amount of air is trapped in the pores, rendering the soil more compressible than expected in the beginning of the subsequent compression process.

Compressive and Shearing Behaviors

Experimental Setup

A laboratory testing program was designed to investigate the deformation behavior of the unsaturated silt at different matric suctions. The experiments were conducted on an improved double cell triaxial apparatus by GDS-HUKUST, in which matric suction was controlled by the axis translation technique (Hilf 1956). Pore air pressure and pore water pressure were applied at the top and bottom of the sample, respectively. Stepper motor–driven regulators were used to control pore air pressure, pore water pressure, cell pressure, and deviatoric stress, and the cell pressure was maintained by air pressure. All experimental data were recorded continuously by a computer.

A new system was introduced to accurately measure the total volumetric change of the unsaturated soil sample (Ng et al. 2002). The system introduced a *twin cell*, in which a differential pressure transducer was introduced to record the differential pressure between the water level in the inner cell and the water level of reference tube. The volume change of the sample was determined using the differential pressure. Further details on this aspect can be found in Ng et al. (2002).

The triaxial apparatus is instrumented with a strain gauge to measure the axial strain. The radial strain is determined from the records of vertical and volumetric deformations. The degree of saturation of the soil sample is determined from the water drainage influx.

Method and Procedure

The tested triaxial sample had a diameter of 50 mm and a height of 100 mm. The sample was statically compacted, in nine layers, to a targeted dry density of $1.6\,\mathrm{g/cm^3}$, with an initial void ratio of approximately 0.7. The interfaces between the different layers were carefully scarified to minimize the inhomogeneity. The compacted samples have practically the same initial density and fabric.

A ceramic disk with an air-entry value of 100 kPa was installed in the pedestal. The sample was saturated using the vacuum method, whereas the ceramic disk and pipelines of the triaxial apparatus were saturated by elevating the cell pressure and back pressure. To ensure the ceramic disk was fully saturated, the saturation procedure was repeated several times.

A series of isotropic compression and shearing tests on the unsaturated compacted silt were performed using the improved suction-controlled double cell triaxial apparatus. All of the applied stress paths in this research are summarized in Table 2. Most of the experiments were involved in several stages, including initial equalization, isotropic compression at constant matric suction, triaxial shearing, and wetting.

Initial Equalization

After installing the sample in the triaxial cell, the deviator stress was set to zero while the cell, pore water, and pore air pressures were applied to achieve the targeted matric suction and mean net stress. Then the sample was left to reach equilibrium at the specified matric suction and mean net stress.

At this stage, identification of the equilibrium state is important, because it may affect the reliability of the subsequent tests. As a general rule, once both the sample volume change and the pore water volume change were less than $0.098\,\mathrm{cm^3/day}$ (0.05% volumetric strain), the equalization stage was assumed to be complete. The duration of equalization stage varied from 15 to 20 days, depending on the value of matric suction applied. Each

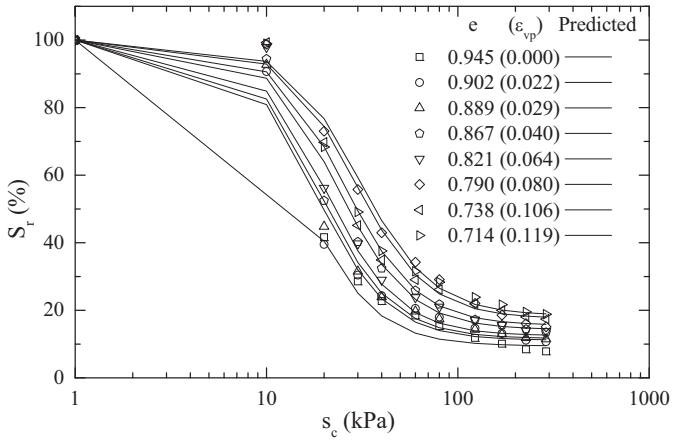

Fig. 2. SWCCs at different initial void ratios

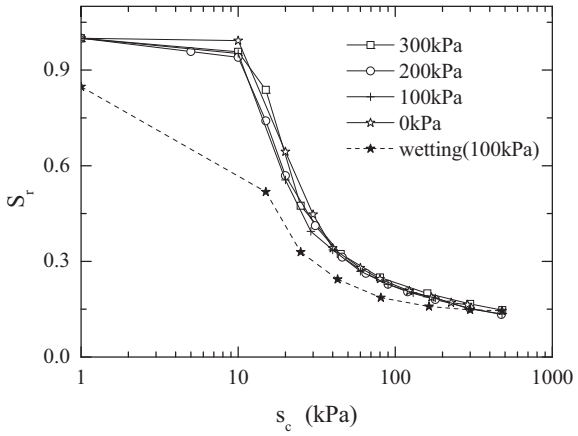

Fig. 3. SWCCs under different vertical net stresses

experimental test started from the equalization stage, with the specified initial mean net stress and matric suction being applied to the sample.

Isotropic Compression at Constant Matric Suction

After the equalization stage, isotropic compression was conducted on the sample under the constant-suction condition. Four matric suctions were adopted in the experiment: $s_c = 0$, 15, 50, and 90 kPa, respectively (as listed in Table 2). During the test, the mean net stress was slowly changed so that the sample attains equilibrium all the time during the compression process. A loading rate of 2 kPa/h was found to be adequate for the tested silt.

Triaxial Shearing

After the sample was isotropically loaded to a specified net confining pressure at a certain matric suction, it was sheared under the drained condition by applying an axial load at a constant compressive strain rate of 0.003%/min. Matric suction was maintained constantly during loading. The shearing stage was terminated when the axial strain increased to 15%, which took approximately 7 days.

Wetting

During the wetting phase, the pore air pressure was reduced until the pore air pressure equaled the pore water pressure. In this stage, the matric suction was decreased very slowly to keep the sample at the equilibrium state all the time.

Results and Discussion

Isotropic Compression at Constant Matric Suction

Fig. 4 shows the variation of specific volume (υ) with the mean effective stress at the different matric suctions, where $\upsilon = 1 + e$, and e = void ratio. The mean effective stress (p') is defined as $p' = p - u_a + S_r(u_a - u_w)$, where p = mean total stress, and u_a and u_w = pore air pressure and pore water pressure, respectively. It can be seen from Fig. 4 that either isotropic compression curves or rebound curves are almost parallel at different matric suctions. That is, on the $\upsilon - \ln p'$ plane, the slopes of compression and rebound curves (i.e., λ and κ, respectively) are independent of the applied matric suction. In a contrast, on the $e - \ln p_{\text{net}}$ plane, λ_{net} decreases with the increase of matric suction.

It is clear that, at matric suction 50 kPa, the recompression curve deviates significantly from the rebound curves. This is because the loading rate (3 kPa/h) in the first compression stage is too fast to make the sample deviate from the equilibrium state.

Table 2. Imposed Stress Paths in Tests

Test no.	p_{net}(kPa)	s_c(kPa)	Shearing	Test period (days)
1	200	15	0.003%/min–15%	30
2	20–400–20–600	50	0.003%/min–15%	35
3	20–200–20–300	90	0.003%/min–15%	34
4	100	90–0	0.003%/min–15%	31

To compare the values of λ and κ to those determined from the fully saturated condition, a consolidation test was performed on the saturated sample using the conventional oedometer. The compression curve is plotted on the $\upsilon - \ln\sigma_v$ plane as shown in Fig. 5, where σ_v = vertical stress. The consolidation test was conducted under the 1D stress state, so that the compression and swelling indexes (C_c and C_s) have to be converted to λ and κ for comparison. To this end, the following relationships can be used: $\lambda = C_c/\ln 10$ and $\kappa = C_s/\ln 10$ (Schofield and Wroth 1968). The result shows that the parameters λ and κ of saturated soil are 0.011 and 0.005, respectively, approximately equal to those of the unsaturated samples at three different matric suctions.

Shearing at Matric Suction of 15 kPa (Test 1)

In Test 1, the sample was sheared under $p_{\text{net}} = 200$ kPa and $s_c = 15$ kPa. The result is shown by the dotted lines in Fig. 6, including the variations of volumetric strain (ε_v), axial strain (ε_1) and radial strain (ε_3) with stress ratio.

Fig. 6(a) shows that, during shearing, the stress ratio increases to the peak value quickly at a small strain and becomes stable with the strain development. At an axial strain of approximately 0.05, σ_1/σ_3 begins to decrease, implying the occurrence of softening. Inspection of Fig. 6(e) reveals that the sample shows apparent dilatant behavior after compaction, and dilation occurs before the peak strength is attained [compare to Fig. 6(a)]. Then the soil hardens further with the development of dilation, and after the peak strength is reached, softening occurs until the soil fails. At the end of the test, a failure surface of the sample was clearly identified [similar to that shown in Fig. 7(f)]. Fig. 6(d) illustrates that, in the beginning of shearing, only small elastic deformation occurs, and the degree of saturation (S_r) decreases very slightly; in sharp contrast, however, S_r decreases significantly after the soil begins to dilate. The decrease in S_r with elastic deformation is an unexpected result,

which is probably due to the fact that the soil was not in equilibrium in the beginning.

Shearing at Matric Suction 50 kPa (Test 2)

In Test 2, the sample experienced loading, unloading, and reloading compression under the isotropic condition at a constant matric suction of 50 kPa. During the compression, the mean net stress was increased at a rate of 3 kPa/h up to 400 kPa, and then decreased at a rate of 2 kPa/h to 20 kPa, and finally increased at a rate of 2 kPa/h to 600 kPa. Experimental observation revealed that the loading rate of 3 kPa/h was so fast that it could not be guaranteed the sample always in equilibrium. Therefore, the loading rate was changed to 2 kPa/h in other tests, and 3 kPa/h was used only for the first compression with 50 kPa suction. A rate of 2 kPa/h was found to be adequate. The isotropic compression/rebound curves are shown by the dashed lines in Fig. 4. The loading rate (3 kPa/h) during the first compression is fast, and the sample may not always be in an equilibrium state; thus, significant deviation from the rebound curve occurs during the reloading stage, as shown in Fig. 4. The conclusion can be confirmed by comparing the results of Test 3. The loading rate of 2 kPa/h was adopted in the isotropic compression/rebound test at 90-kPa matric suction. As shown schematically in Fig. 4(a), the slopes between recompression and rebound curves have almost the same value. It can be concluded that the difference in slopes between recompression and rebound curves at 50-kPa matric suction is due to the loading rate. Subsequently, the sample was sheared at a constant mean net stress of $p_{net} = 600$ kPa and a matric suction of $s_c = 50$ kPa. The results are shown by the dashed lines in Fig. 7.

Clearly, the behavior of the sample is similar to the previous sample (Test 1), which shows softening and dilatant behavior. Unlike the sample in Test 1, the sample in Test 2 shows less dilatancy (compare Fig. 7 to Fig. 6). Similar to the behavior of sand, dilatancy of silt decreases with the increase of mean net stress. Because matric suctions applied in both tests are different, the observed trend is qualitative only. The peak strength of the sample in Test 2 is larger than that in Test 1 due to the larger matric suction and mean net stress. As shown in Fig. 7(c), the strength of the sample decreased suddenly after approximately 0.1 deviatoric strain. That is because a clear failure surface occurred through the sample [Fig. 7(f)].

Shearing at Matric Suction 90 kPa (Test 3)

In Test 3, the isotropic compression test was conducted at a constant matric suction of 90 kPa. The mean net stress first increased at a rate of 2 kPa/h to 200 kPa, then decreased at a rate of 2 kPa/h to 20 kPa, and finally increased at a rate of 2 kPa/h to 300 kPa. The isotropic compression/rebound curves are shown by the dashed lines in Fig. 4.

After the recompression stage, the sample was sheared under a constant mean net stress of $p_{net} = 300$ kPa and a matric suction of $s_c = 90$ kPa. The experimental results are given by the dashed lines in Fig. 8. The behavior of the sample is similar to those of Tests 1 and 2, which show clear softening and dilatant effects. Compared to Test 2 (Fig. 7), the peak strength is smaller, whereas dilatancy is more significant. Inspection of Fig. 8 reveals that the strength of the sample decreases after the peak strength (similar to Figs. 6 and 7) and then increases again, until the critical state is reached.

Wetting Test at Mean Net Stress 100 kPa (Test 4)

In Test 4, the initial equalization state was arrived at $s_c = 90$ kPa and $p_{net} = 100$ kPa. After the equalization state, the sample was wetted at the constant mean net stress of 100 kPa. The matric suction was decreased at a rate of 0.1875 kPa/h to 0 kPa. Perhaps

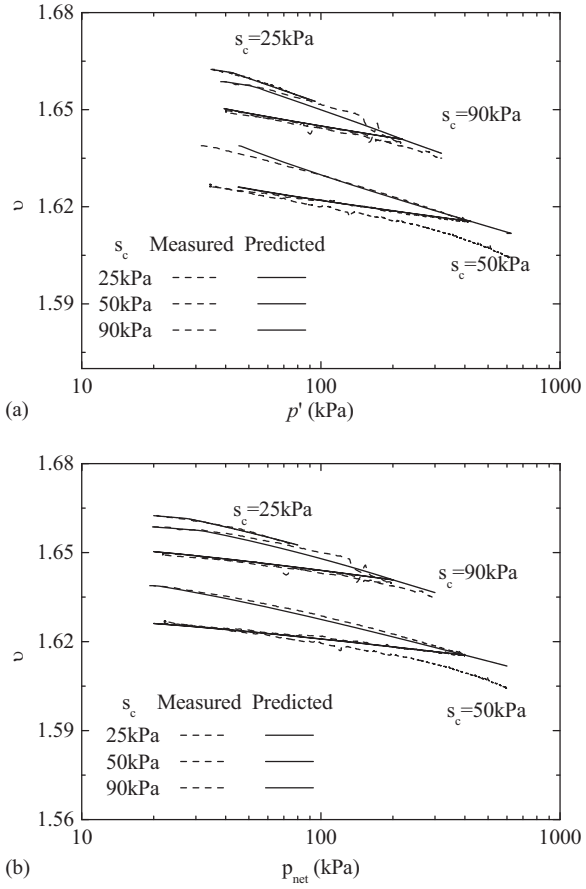

Fig. 4. Isotropic compression at different matric suctions: (a) specific volume versus mean effective stress; (b) specific volume versus mean net stress

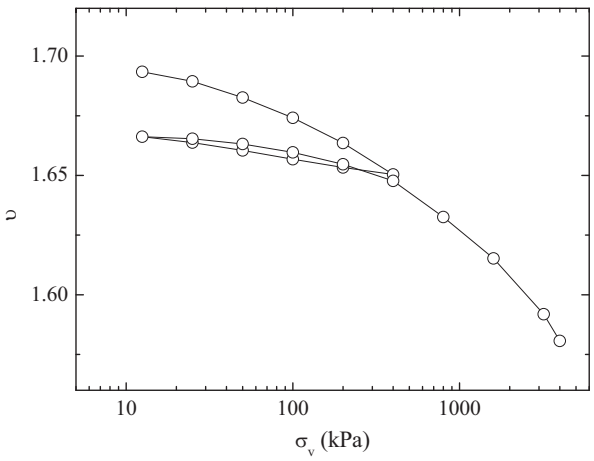

Fig. 5. The 1D compression curve of the fully saturated sample

because the rate was too fast, the sample had not reached equilibrium when the matric suction decreased to 0 kPa. Then, the matric suction was maintained at 0 kPa, and the sample was left to attain equilibrium. After the equilibrium state was reached, the sample was sheared at $s_c = 0$ kPa and $p_{net} = 100$ kPa. During the wetting process, no collapse phenomenon occurred. The results are shown by the dashed lines in Fig. 9. The strength of the sample is smaller

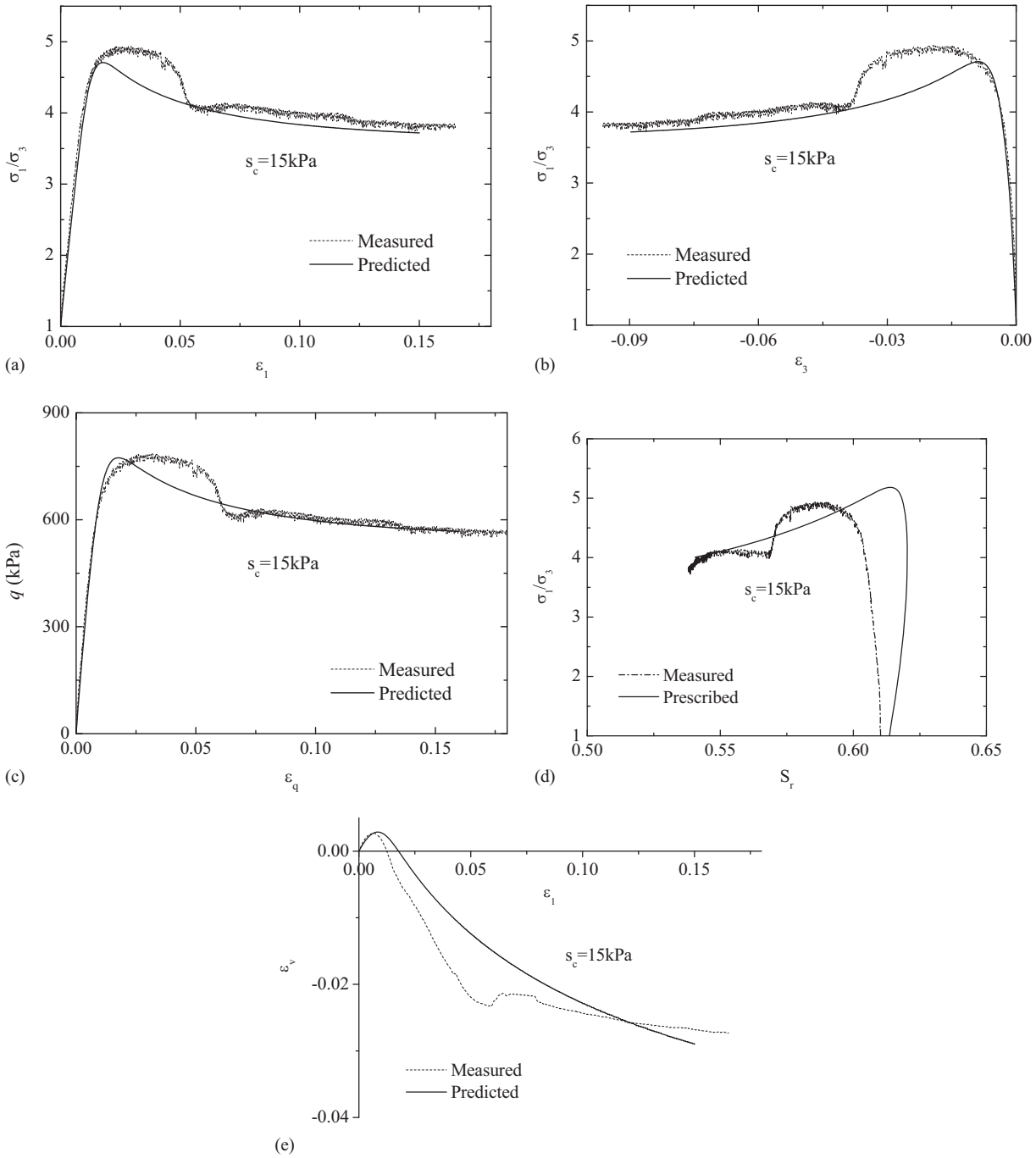

Fig. 6. Results for 15-kPa suction: (a) stress ratio versus axial strain; (b) stress ratio versus radial strain; (c) deviatoric stress versus deviatoric strain; (d) stress ratio versus saturation; (e) volumetric strain versus axial strain

compared to other tests. The phenomena of dilatancy and softening are more prominent. As strain developed, the critical state was finally reached.

Main Features of Unsaturated Silt Behavior: Summary

Based on the experimental results presented earlier, the main features of the unsaturated silt behavior are summarized as follows:

1. The hardening effect of the soil becomes more significant with increases in both the confining pressure and the matric suction. The critical state appears when the volume change and deviator stress approach some stable values.
2. During the shearing process, the volumes of the samples increased after a slight contraction. Dilatancy and softening behavior are observed in the stress-strain relationship of the unsaturated silt. In general, the behavior of the soil progressively evolves from dilation to contraction, with increasing confining net pressure, until the dilatancy completely disappears, illustrating a transition from brittle behavior to ductile behavior (Verdugo and Ishihara 1996).
3. The dilatancy depends upon the matric suction, i.e., the higher the matric suction is, the more significant the dilatancy is. Such a trend is opposite that of the effect of the confining stress on the

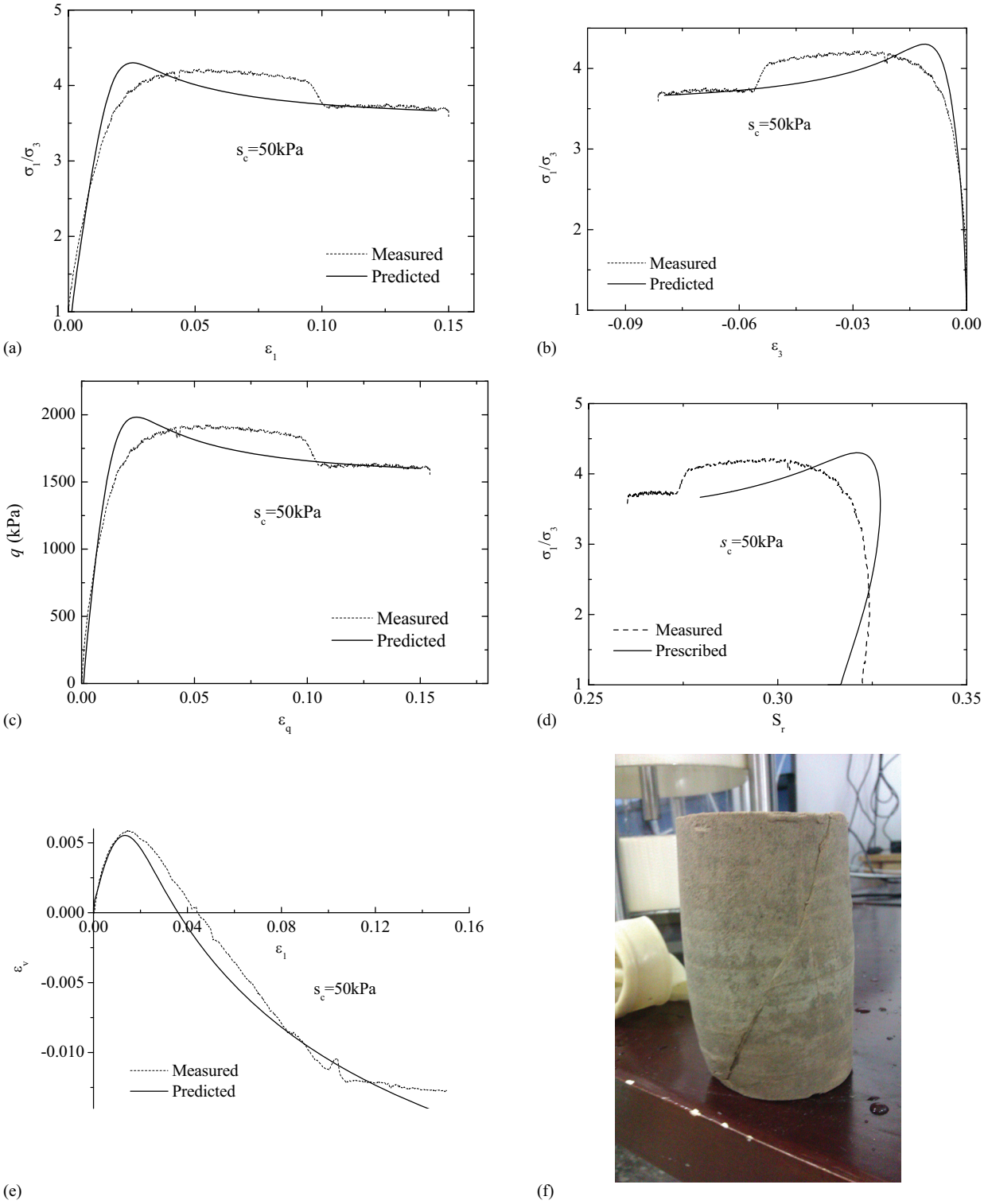

Fig. 7. Results for 50-kPa suction: (a) stress ratio versus axial strain; (b) stress ratio versus radial strain; (c) deviatoric stress versus deviatoric strain; (d) stress ratio versus saturation; (e) volumetric strain versus axial strain; (f) photo of the silt sample after shearing

dilatancy. That is, the brittleness of the soil increases with the matric suction, which favors dilatancy. These features are consistent with previous experimental results (Ng and Zhou 2005).

4. There is a characteristic point in the stress-strain relationship at which the soil behavior transitions from contraction to dilation. The transition point depends upon the initial density of the sample and the confining pressure. At the same initial void ratio, the dilatancy stress ratio increases with the confining pressure (Manzari and Dafalias 1997).
5. Dilatancy in the unsaturated silt occurs before the peak strength is reached. That is, the strength can increase further with the development of dilatancy.

Noticeably, the tests were conducted on the samples with the same initial conditions, and hence the effect of void ratio was not

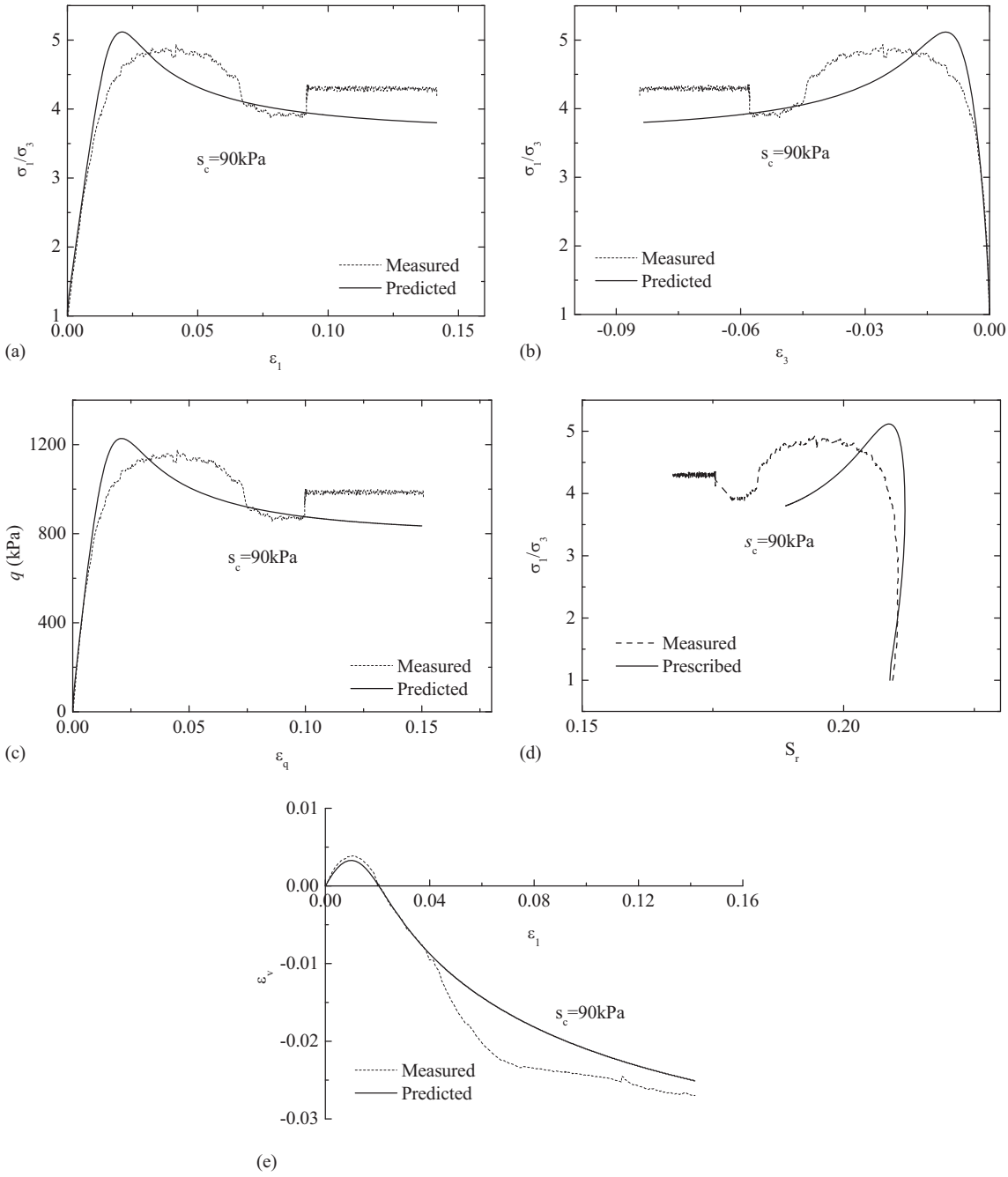

Fig. 8. Results for 90-kPa suction: (a) stress ratio versus axial strain; (b) stress ratio versus radial strain; (c) deviatoric stress versus deviatoric strain; (d) stress ratio versus saturation; (e) volumetric strain versus axial strain

examined. However, according to the experimental results of sandy soils, dilatancy develops in dense samples versus contraction in loose samples. At a certain stress level, the dilatancy stress ratio increases with the increase of void ratio. When the dilatancy state coincides with the critical state, dilatancy no longer exists (Verdugo and Ishihara 1996; Yoshimine et al. 1999).

Constitutive Model of Dilatant Soils

Based on the previous experimental results, a constitutive model is developed here for the unsaturated dilatant soils within the framework of critical state soil mechanics.

Stress State Variables

To develop the stress-strain relationship, the average skeleton stress (σ'_{ij}) (Jommi 2000) and the matric suction (s_c) are introduced, which are defined, respectively, by

$$\sigma'_{ij} = (\sigma_{ij} - u_a\delta_{ij}) + S_r(u_a - u_w)\delta_{ij} \quad (1)$$

$$s_c = u_a - u_w \quad (2)$$

where σ_{ij} = total stress tensor, and δ_{ij} is the unit tensor.

At the triaxial stress state

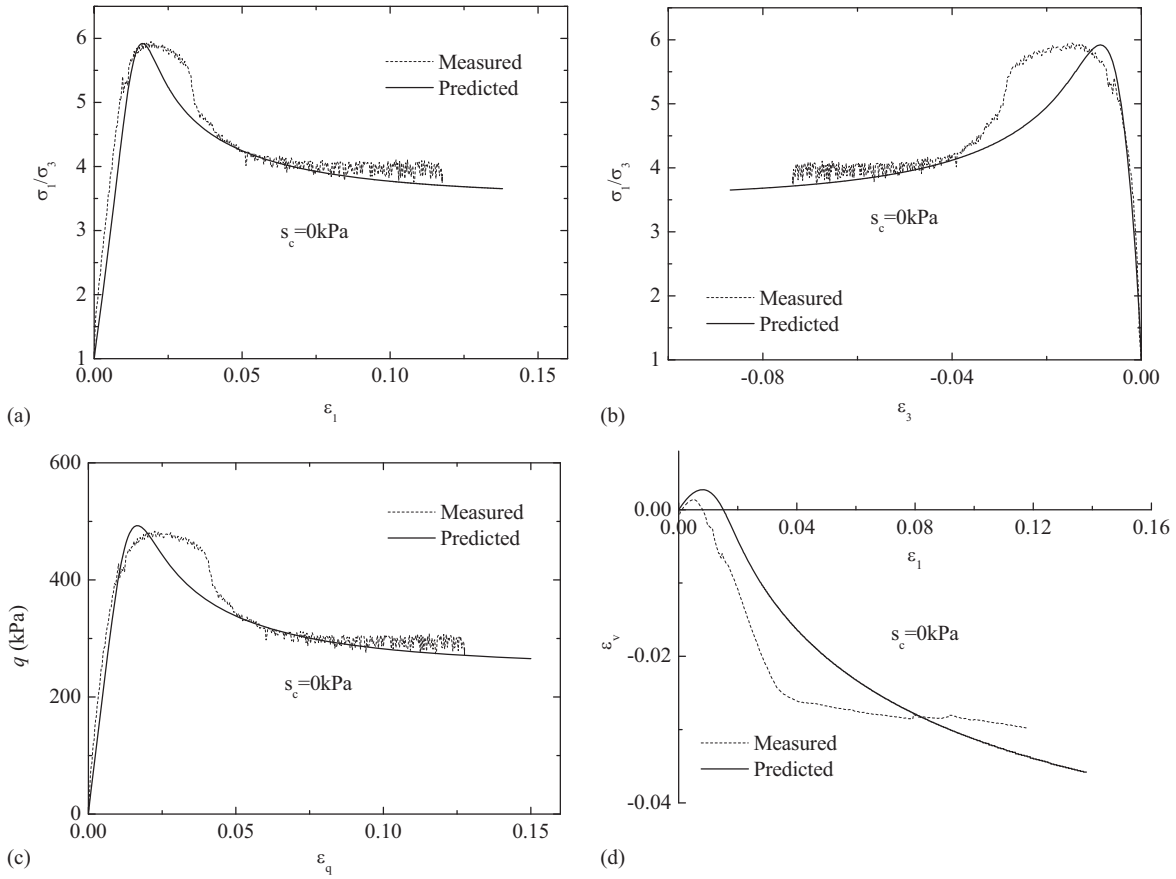

Fig. 9. Results for 0-kPa suction: (a) stress ratio versus axial strain; (b) stress ratio versus radial strain; (c) deviatoric stress versus deviatoric strain; (d) volumetric strain versus axial strain

$$p' = \frac{\sigma'_{ii}}{3} = (p - u_a) + S_r(u_a - u_w) \tag{3}$$

$$q = \sigma'_1 - \sigma'_3 \tag{4}$$

where p = mean total stress, and σ'_{ij} is defined by Eq. (1) and simply Bishop's *effective* stress of unsaturated soils (Bishop 1959), with parameter χ equal to the degree of saturation (S_r). Noticeably, the generalized stress variables (σ'_{ij}, s_c) are work conjugated to the generalized strain variables (ε_{ij}, S_r).

Yield Surface

The stress-strain relationship is developed by generalizing the modified Cam clay model (Roscoe and Burland 1968), in which the yield function is given by

$$f = q^2 + M^2 p'(p' - p_c) \tag{5}$$

where p_c = preconsolidation pressure. At full saturation, p_c is a function of plastic volumetric strain and plastic deviatoric strain, i. e., $p_c = p_{c0}(\varepsilon_v^p, \varepsilon_q^p)$. Under partially saturated conditions, p_c depends upon matric suction and the degree of saturation as well as the plastic volumetric strain and the plastic deviatoric strain.

Hence, it is suggested herein that the critical state line of unsaturated soil is the same as that of its saturated counterpart, and the failure line is simply given by $q = Mp'$, where M is independent of the matric suction or the degree of saturation (Lu and Likos 2006).

Hardening Rule

It has been well recognized that the soil can harden further after dilation occurs. Therefore, in developing the hardening rule, the effect of plastic deviatoric strain has to be taken into account (Bolzon et al. 1996). Based on the aforementioned experimental results, the soil becomes stiffer when the matric suction is larger, and accordingly, the hardening effect of plastic deviatoric strain becomes more evident. Hence, it is proposed herein that

$$p_c = p_{c0} \exp\left(\frac{\upsilon}{\lambda - \kappa}\varepsilon_v^p + \frac{\beta\upsilon}{\lambda - \kappa}\varepsilon_q^p\right) \cdot h(s_c, S_r, \varepsilon_v^p) \tag{6}$$

where p_{c0} = initial preconsolidation pressure, and parameter β = proportional coefficient of the hardening effect of the plastic deviatoric strain, which is a function of the suction and degree of saturation, and it is explicitly assumed that

$$\beta = \beta_0 \cdot \left[1 + \frac{(1 - S_r)s_c}{1 - S_r^{\text{irr}}}\right] \tag{7}$$

As described by Eqs. (6) and (7), when $(1 - S_r)s_c$ increases, β increases, and the dilatancy of the soil becomes more apparent. When $\beta_0 = 0$, Eq. (6) degenerates into the hardening rule for clayey soils. When the suction is zero, $\beta = \beta_0$ and $h = 1$, and the

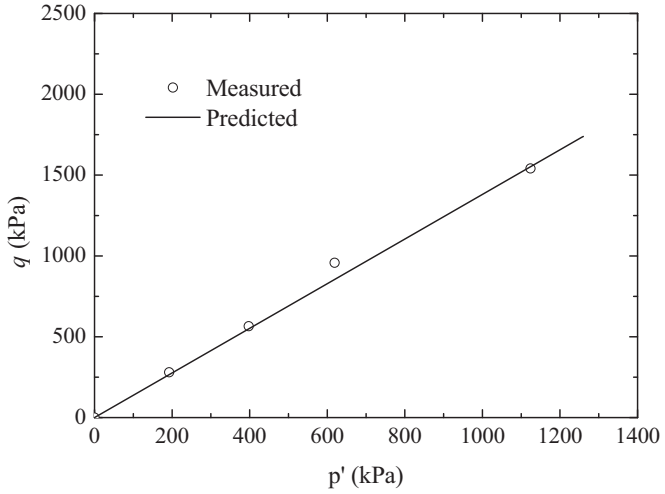

Fig. 10. Critical state line

model degenerates into the one for the saturated silt/sand. Variable h is a correction function, which accounts for the hardening effect of unsaturation, and it is assumed to be a function of s_c, S_r, and ε_v^p

$$h(\varepsilon_v^p, S_r, s_c) = r - (r-1)\exp\left[-m\left\langle 1 - \frac{\varepsilon_v^p}{\varepsilon_{v,\max}^p}\right\rangle \frac{(1-S_r)s_c}{(1-S_r^{\text{irr}})}\right] \quad (8)$$

where r and m = material constants; $\varepsilon_{v,\max}^p$ = maximum plastic volumetric strain; and S_r^{irr} = residual degree of saturation. $\langle\rangle$ is a Macaulay bracket, defined as $\langle x\rangle = xH(x)$, where $H(x)$ = Heaviside function. $(1-S_r)s_c$ is introduced to characterize collectively the hardening effect of unsaturation, which can represent the quantity of meniscus water rings. Remarkably, at the specified matric suction, the value of $(1-S_r)s_c$ depends *uniquely* upon the pattern of moisture distribution in the pores, i.e., upon the hydraulic history that the soil experienced.

From the proposed hardening function, h increases with the decrease in saturation or increase in suction, and approaches a certain value when $S_r \to S_r^{\text{irr}}$ or $s_c \to +\infty$. When the soil is fully saturated, the effect of capillarity on the hardening vanishes, i.e., $h = 1.0$ when $S_r = 100\%$. In addition, the effect of S_r and s_c on the preconsolidation pressure diminishes gradually with increasing ε_v^p. When ε_v^p reaches the maximum ($\varepsilon_{v,\max}^p$), the influence of S_r and s_c on the preconsolidation pressure disappears, implying that the soil is very dense and the capillary effect can be negligible.

Clearly, the proposed function can transition from saturated state to unsaturated state smoothly, so that both states can be described in a single framework. In addition, it can be numerically implemented in a straightforward way.

Elastoplastic Stress-Strain Relationship

The increments of elastic volumetric strain and deviatoric strain are given by

$$d\varepsilon_v^e = \frac{\kappa dp'}{vp'}, \quad d\varepsilon_q^e = \frac{dq}{3G} \quad (9)$$

where G = shear modulus.

Flow Rule

For dilative soils, the associated flow rule will overestimate the dilatancy. Therefore, the nonassociated flow rule is adopted in this model. Here, it is assumed that

$$d = \frac{d\varepsilon_v^p}{d\varepsilon_q^p} = M\exp(n\varphi) - \eta \quad (10)$$

where the slope of dilatancy state line is $M_p = M\exp(n\varphi)$, and n = nondimensional parameter, which denotes the contribution of state parameter to the dilatancy stress ratio. A larger value of n implies that the dilatancy state is further away from the critical state and dilatancy of the material is more prominent. As shown in Eq. (10), with the development of dilatancy, the dilatancy state line approaches the critical state line and coincides with the critical state line when the soil reaches the critical state. Noticeably, Eq. (10) can be considered as a specific case of the general expression proposed by Dafalias et al. (2005).

Inspection of Eq. (10) reveals that soil contraction appears in the early beginning of a shearing process. When the dilatancy point is reached ($\eta = M_p$), the plastic volumetric deformation is zero. With the shearing process, the plastic volumetric deformation becomes negative, i.e., the soil dilates between the dilatancy state point and failure point. With the development of dilatancy, the soil hardens further and finally softens. When the intersection between critical state line and elliptic yield surface (failure point) is attained, the soil reaches the final failure state (critical state).

The incremental plastic deviatoric strain is calculated by $d\varepsilon_q^p = d\lambda(\partial f/\partial q)$, where $d\lambda$ = plastic multiplier that can be determined based on the consistency condition. The incremental plastic volumetric strain can be obtained through the nonassociated flow rule, i.e., $d\varepsilon_v^p = d\varepsilon_q^p \cdot d$.

Effect of Deformation on the SWCC

In general, the change in the degree of saturation has two contributions: one is the change in the amount of pore water due to seepage or dissipation, and the other is due to the change in the pore volume, namely

$$dS_r = d\left(\frac{V_w}{V_v}\right) = \frac{dV_w}{V_v} - \left(\frac{V}{V_v}\right)\left(\frac{V_w}{V_v}\right)\left(\frac{dV_v}{V}\right) \quad (11)$$

Neglecting the effect of elastic deformation, Eq. (11) can be cast into

$$dS_r = dS_r|_{d\varepsilon_v=0} + \frac{S_r}{n_0}d\varepsilon_v^p \quad (12)$$

where n_0 = porosity. According to Wei and Dewoolkar (2006), the first term of the right-hand side can be described by

$$dS_r|_{d\varepsilon_v=0} = \frac{-ds_c}{K_p(s_c, S_r, \hat{n})} \quad (13)$$

where $\hat{n}$ = hydraulic loading direction, and its value assumes 1 (or –1) for drying (or wetting); K_p = negative slope of the current SWCC (either scanning or boundary), which is a function of s_c, S_r, and $\hat{n}$, given by

$$K_p(s_c, S_r, \hat{n}) = \bar{K}_p(S_r, \hat{n}) + \frac{c|s_c - \bar{s}_c(S_r, \hat{n})|}{r(S_r) - |s_c - \bar{s}_c(S_r, \hat{n})|} \quad (14)$$

where $\bar{K}_p(S_r, \hat{n})$ = negative slope of the *corresponding main boundary*, which is the main drying boundary if $\hat{n} = 1$ or the main wetting

boundary if $\hat{n} = -1$; c = positive material parameter which is used to describe the scanning behavior; $\bar{s}_c(S_r, \hat{n})$ = matric suction value on the corresponding main boundary curve, i.e., $\bar{s}_c(S_r, 1) = \kappa_{DR}(S_r)$ for drying and $\bar{s}_c(S_r, -1) = \kappa_{WT}(S_r)$ for wetting, where $\kappa_{DR}(S_r)$ and $\kappa_{WT}(S_r)$ describe the main drying and wetting boundaries, respectively; and $r(S_r)$ = current size of the bounding zone, i.e., $r(S_r) = \kappa_{DR}(S_r) - \kappa_{WT}(S_r)$. In the hysteretic SWC relationship proposed by Wei and Dewoolkar (2006), the recoverable part of the moisture content was ignored.

The following SWCC model by Feng and Fredlund (1999) is adopted to describe the main boundaries:

$$\kappa_k(S_r) = b_k \left(\frac{1 - S_r}{S_r - S_r^{\text{irr}}} \right)^{1/d_k}, \; k = \text{DR, WT} \tag{15}$$

where b_k and d_k = positive material parameters, and assume different values for wetting and drying. Experimental results of SWC suggest that the skeletal deformation changes the position of the SWCC only, whereas the shape of the curve remains practically unchanged. Thus, for simplicity, it is proposed that

$$b_k = b_k^0 + \alpha_k \varepsilon_v^p, \; d_k = d_k^0 \tag{16}$$

where b_k^0, d_k^0, and α_k = curving-fitting parameters, and k = DR (for drying) and WT (for wetting).

Due to a lack of experimental data, for simplicity, it is assumed that parameter c is a constant, independent of the skeletal deformation. Now, for deforming soils, Eq. (14) can be replaced by

$$K_p(\varepsilon_v^p, s_c, S_r, \hat{n}) = \bar{K}_p(\varepsilon_v^p, S_r, \hat{n}) + \frac{c|s_c - \bar{s}_c(\varepsilon_v^p, S_r, \hat{n})|}{r(\varepsilon_v^p, S_r) - |s_c - \bar{s}_c(\varepsilon_v^p, S_r, \hat{n})|} \tag{17}$$

Fig. 2 illustrates the effect of the plastic volumetric strain on the SWCC. It can be seen that, whereas the theoretical simulations agree reasonably well with the experimental results, the model is capable of capturing the main features of the SWCC of deformable soils. The model prediction about the effect of plastic volumetric strain on the wetting curves was not shown due to the lack of experimental results.

Model Calibration

The proposed model avoids using the loading-collapse (LC) yield curve as in the traditional framework, and introduces the matric suction and degree of saturation into the hardening function as independent variables. In addition, parameters n and β_0 are introduced to address the dilatant and softening effect of the soils. The constitutive parameters can be divided into the following three groups:

1. Group 1: Conventional constitutive parameters—$\lambda, \kappa, M, G, n, \beta_0$
2. Group 2: SWC parameters—b_{DR}^0, b_{WT}^0, d_{DR}^0, d_{WT}^0, S_r^{irr}, c
3. Group 3: Coupling parameters—α_{DR}, α_{WT}, r, m, $\varepsilon_{v,\max}^p$

Parameters λ and κ can be obtained based on the aforementioned isotropic compression and rebound tests. Based on the experimental results in Fig. 4, it can be determined that $\kappa = 0.005$ and $\lambda = 0.011$, both of which are independent of the matric suctions. Based on the results of triaxial shear tests, shear modulus (G) is approximately 8 MPa. In general, G may change with suction or saturation. As an approximation, however, it is assumed here that G is independent of the matric suction.

The critical states of the soil samples at different matric suctions and degrees of saturation are shown in Fig. 10. It can be seen that all critical state points approximately stay on a straight line, showing that the critical state is independent of the hydraulic state of soil. By fitting the test data, the slope of the critical state line is obtained, i.e., $M = 1.38$. Using $M_p = M \exp(n\varphi)$, $n = 1.4$ is obtained, by fitting the measured dilatancy points of all triaxial shear tests.

Parameters b_{DR}^0, b_{WT}^0, d_{DR}^0, d_{WT}^0, and S_r^{irr} are determined, via the curve-fitting procedure, using the two boundary curves in Fig. 3. Given the two boundary curves, c is determined by fitting the theoretical simulation of a primary scanning curve with the measured one (Wei and Dewoolkar 2006).

Among the parameters in Group 3, r, m, and $\varepsilon_{v,\max}^p$ can be determined by measuring the variation of preconsolidation pressure with the matric suction or degree of saturation during a drying process; parameters α_{DR} and α_{WT}, which represent the influence of plastic deformation on the SWCC, can be obtained by comparing the SWCCs under deformed and undeformed conditions. According to the experimental results in Fig. 2, one can obtain $\alpha_{DR} = 127$ kPa. All the model parameters are summarized in Tables 3–5.

Table 3. Model Parameters for Strain–Stress Relationship

Parameter	Value
λ	0.011
κ	0.005
G (kPa)	80,000
M	1.38
n	1.4
β_0	0.4

Table 4. Model Parameters for SWCC

Parameter	Value
b_{DR}^0 (kPa)	22.11
d_{DR}^0	3.11
b_{WT}^0 (kPa)	12.73
d_{WT}^0	1.80
S_r^{irr}	14.9%
c (kPa)	100

Table 5. Model Parameters for Coupling

Parameter	Value
r	5.0
m	0.0236
α_{DR} (kPa)	127
α_{WT} (kPa)	35

Model Performance

The new model is used to simulate the experimental results, as shown by the solid lines in Figs. 6–9. From the simulation results, one can see that the model is capable of capturing the main features of the hydraulic and mechanical behavior of unsaturated silt. The new model can effectively describe the coupling of capillary hysteresis and skeletal deformation. The effect of matric suction on soil hardening and dilatancy is also properly addressed. However, the proposed model could not predict the cyclic behavior of unsaturated silt effectively.

In Figs. 6–9, it is clear that the proposed model can describe reasonably well the dilatancy and softening behavior of unsaturated silt. Although the model predictions of stress-strain relationships deviate from the measurements in the beginning of the softening

stage, the model can well capture the critical state behavior of the soil.

Figs. 6(d)–9(d) show that the volume change is underestimated in the later stage of the shearing process. Despite this discrepancy, the model simulations agree well with the measurements. Remarkably, the degree of saturation increases during the shearing contraction process, then decreases when the dilatancy occurs, and this feature has been well captured by the proposed model, as illustrated in Figs. 6(d) and 8(d).

Conclusions

The hydraulic and mechanical behavior of the statically compacted silt was studied in this paper. Based on the experimental results, it is shown that the key factor that influences the water-retention capacity is the void ratio, and the stress state can influence the SWC only through changing the void ratio (i.e., the deformation).

A series of triaxial tests were performed to study the yielding and plastic flow at various suctions. Particular attention was given to the volume changes. It was found that, during a shearing process, the volumetric strain transforms from positive (contraction) to negative (dilation). A unified elastoplastic model coupling the hydraulic and mechanical behavior of unsaturated soils is proposed in the framework of critical state soil mechanics. The model introduces the state parameter into the dilatancy relationship to account for the effect of initial condition (including void ratio, stress level, and unsaturation). The behavior of the same soil with different initial conditions can be simulated using only one set of material parameters. A formulation of the nonassociated flow rule, similar to that deduced from sand behavior, is proposed to predict volume deformation during the shear process of the silt.

In the new model, the SWCC is introduced not only to describe the capillary hysteresis in the unsaturated soils experiencing arbitrary wetting/drying cycles, but also to characterize the effect of hydraulic history on the skeletal deformation via a hardening function. The hardening rule of the preconsolidation pressure considers the effect of plastic deviatoric strain and the effect of matric suction on dilatancy. The effect of the plastic volumetric strain on water-retention behavior is also taken into account. According to the simulation of the test results, the model can be verified to reflect the deformation features of unsaturated silt accurately.

Acknowledgments

The research was supported by the National Key Basic Research Program of China under Grant 2012CB026102, the Natural Science Foundation of China under Grant 51239010, and the Natural Science Foundation of Guangxi under Grant 2012GXNSFGA060001.

Notation

The following symbols are used in this paper:

b^0_{DR}, b^0_{WT}, d^0_{DR}, d^0_{WT} = positive material parameters of Feng and Fredlund model;
C_c, C_s = compression, swelling indexes;
c = positive material parameter used to describe the scanning behavior;
$d\varepsilon^e_v$, $d\varepsilon^e_q$ = increments of elastic volumetric, deviatoric strains;
$d\lambda$ = plastic multiplier;
e = void ratio;
G = shear modulus;
h = hardening function;
K_p = negative slope of the current SWCC;
$\bar{K}_p(S_r, \hat{n})$ = negative slope of the corresponding main boundary;
M, M_p = slopes of critical state line, dilatancy state line;
m, r = material parameters of the hardening effect of unsaturation;
n = nondimensional parameter describing the contribution of state parameter on the dilatancy stress ratio;
n_0 = porosity of soil;
$\hat{n}$ = hydraulic loading direction;
p, p', p_{net} = mean total, effective, net stresses;
pc, p_{c0} = preconsolidation pressures of unsaturated soil, saturated soil;
q = deviatoric stress;
$r(S_r)$ = current size of the bounding zone;
s_c = matric suction;
$\bar{s}_c(S_r, \hat{n})$ = matric suction value on the corresponding main boundary curve;
S_r = degree of saturation;
S^{irr}_r = residual degree of saturation;
u_a, u_w = air, water pressures;
V = total volume of soil element;
V_w, V_v = volumes of water, void in a soil element;
v = specific volume;
α_{DR}, α_{WT} = material parameters describing the effect of deformation on the SWCCs;
β, β_0 = proportional coefficients of the hardening effect of the plastic deviatoric strain of unsaturated soil, saturated soil;
δ_{ij} = unit tensor;
ε_v = volumetric strain;
ε_{ij} = strain tensor;
$\varepsilon^p_v, \varepsilon^p_q$ = plastic volumetric, plastic deviatoric strains;
$\varepsilon^p_{v,max}$ = maximum plastic volumetric strain;
$\varepsilon_1, \varepsilon_3$ = principal strains;
η = stress ratio;
κ = slope of rebound curve in the $v - \ln p'$ plane;
$\kappa_{DR}(S_r), \kappa_{WT}(S_r)$ = matric suctions at main drying and wetting boundaries;
λ, λ_{net} = slopes of compression curves in the $v - \ln p'$ plane, $v - \ln p_{net}$ plane;
σ_v = vertical stress;
$\sigma'_{ij}, \sigma_{ij}$ = average skeleton, total stress tensors;
σ_1, σ_3 = principal net stresses;
χ = weight factor for effective stress variable; and
φ = state parameter.

References

Alonso, E. E., Gens, A., and Josa, A. (1990). "A constitutive model for partially saturated soils." *Géotechnique*, 40(3), 405–430.

Alonso, E. E., Iturralde, E. O., and Romero, E. (2007). "Dilatancy of coarse granular aggregates." *Proc., 2nd Int. Conf. on Mechanics of Unsaturated Soils, Experimental Unsaturated Soil Mechanics*, Springer, Heidelberg, Germany, 119–135.

Been, K., and Jefferies, M. G. (1985). "A state parameter for sands." *Géotechnique*, 35(2), 99–112.
Bishop, A. W. (1959). "The principle of effective stress." *Teknisk Ukeblad*, 106, 859–863.
Bolzon, G., Schrefler, B. A., and Zienkiewicz, O. C. (1996). "Elastoplastic soil constitutive laws generalized to partially saturated states." *Géotechnique*, 46(2), 279–289.
Boyd, J. L., and Sivakumar, V. (2011). "Experimental observations of the stress regime in unsaturated compacted clay when laterally confined." *Géotechnique*, 61(4), 345–363.
Chiu, C. F., and Ng, C. W. W. (2003). "A state-dependent elasto-plastic model for saturated and unsaturated soils." *Géotechnique*, 53(9), 809–829.
Cui, Y. J., and Delage, P. (1996). "Yielding and plastic behaviour of an unsaturated compacted silt." *Géotechnique*, 46(2), 291–311.
Dafalias, Y. F., Papadimitriou, A. G., Li, X. S., and Manzari, M. T. (2005). "Generic constitutive ingredients in CSSM models for sands." *Proc, Int. Workshop on Modern Trends in Geomechanics Experimental*, Springer, Heidelberg, Germany, 26–29.
D'onza, F., et al. (2011). "Benchmark of constitutive models for unsaturated soils." *Géotechnique*, 61(4), 283–302.
Feng, M., and Fredlund, D. G. (1999). "Hysteresis influence associated with thermal conductivity sensor measurements." *52nd Canadian Geotechnical Conf. and Unsaturated Soil Group, Proceeding from Theory to the Practice of Unsaturated Soil Mechanics*, Canadian Geotechnical Society, Richmond, BC, Canada, 651–657.
Gallipoli, D., Gens, A., Sharma, R., and Vaunat, J. (2003). "An elasto-plastic model for unsaturated soil incorporating the effects of suction and degree of saturation on mechanical behaviour." *Géotechnique*, 53(1), 123–135.
Hilf, J. W. (1956). "An investigation of pore-water pressure in compacted cohesive soils." *Technical Memorandum 654*, U.S. Dept. of Interior, Bureau of Reclamation, Denver.
Jommi, C. (2000). "Remarks on the constitutive modelling of unsaturated soils." *Proc., Int. Workshop on Unsaturated Soils*, Experimental Evidence and Theoretical Approaches in Unsaturated Soils, Balkema, the Netherlands, 139–153.
Khalili, N., Habte, M. A., and Zargarbashi, S. (2008). "A fully coupled flow deformation model for cyclic analysis of unsaturated soils including hydraulic and mechanical hystereses." *Comput. Geotech.*, 35(6), 872–889.
Li, X. S., and Dafalias, Y. F. (2000). "Dilatancy for cohesionless soils." *Géotechnique*, 50(4), 449–460.
Liu, C., and Muraleetharan, K. K. (2012a). "Coupled hydro-mechanical elastoplastic constitutive model for unsaturated sands and silts. I: Formulation." *Int. J. Geomech.*, 10.1061/(ASCE)GM.1943-5622.0000146, 239–247.
Liu, C., and Muraleetharan, K. K. (2012b). "Coupled hydro-mechanical elastoplastic constitutive model for unsaturated sands and silts. II: Integration, calibration, and validation." *Int. J. Geomech.*, 10.1061/(ASCE)GM.1943-5622.0000147, 248–259.
Lu, N., and Likos, W. J. (2006). "Suction stress characteristic curve for unsaturated soil." *J. Geotech. Geoenviron. Eng.*, 10.1061/(ASCE)1090-0241(2006)132:2(131), 131–142.
Maatouk, A., Leroueil, S., and Rochelle, P. L. (1995). "Yield and critical state of a collapsible unsaturated silty soil." *Géotechnique*, 45(3), 465–477.
Manzari, M. T., and Dafalias, Y. F. (1997). "A critical state two-surface plasticity model for sands." *Géotechnique*, 47(2), 255–272.
Miller, G. A., Khoury, C. N., Muraleetharan, K. K., Liu, C., and Kibbey, T. C. G. (2008). "Effects of soil skeleton deformations on hysteretic soil water characteristic curves: Experiments and simulations." *Water Resour. Res.*, 44(5), W00C06.
Ng, C. W. W., Zhan, L. T., and Cui, Y. J. (2002). "A new simple system for measuring volume changes in unsaturated soils." *Can. Geotech. J.*, 39(3), 757–764.
Ng, C. W. W., and Zhou, R. Z. B. (2005). "Effects of soil suction on dilatancy of an unsaturated soil." *Proc., 16th Int. Conf. on Soil Mechanics and Geotechnical Engineering*, Vol. 2, Millpress, Rotterdam, the Netherlands, 559–562.
Ng, W. W. C., and Pang, Y. W. (2000). "Influence of stress state on soil-water characteristics and slope stability." *J. Geotech. Geoenviron. Eng.*, 10.1061/(ASCE)1090-0241(2000)126:2(157), 157–166.
Roscoe, K. H., and Burland, J. B. (1968). "On the generalized stress-strain behavior of 'wet' clay." *Eng. Plast.*, 535–609.
Schofield, A. N., and Wroth, C. P. (1968). *Critical state soil mechanics*, McGraw-Hill, London.
Sheng, D., Sloan, S. W., and Gens, A. (2004). "A constitutive model for unsaturated soils: Thermomechanical and computational aspects." *Comput. Mech.*, 33(6), 453–465.
Sun, D. A., Sheng, D., and Sloan, S. W. (2007a). "Elastoplastic modelling of hydraulic and stress-strain behaviour of unsaturated soils." *Mech. Mater.*, 39(3), 212–221.
Sun, D. A., Sheng, D., and Xu, Y. (2007b). "Collapse behaviour of unsaturated compacted soil with different initial densities." *Can. Geotech. J.*, 44(6), 673–686.
Tamagnini, R. (2004). "An extended Cam-clay model for unsaturated soils with hydraulic hysteresis." *Géotechnique*, 54(3), 223–228.
Toll, D. G. (1990). "A framework for unsaturated soil behaviour." *Géotechnique*, 40(1), 31–44.
Verdugo, R., and Ishihara, K. (1996). "The steady state of sandy soils." *Soils Found.*, 36(2), 81–91.
Wei, C., and Dewoolkar, M. M. (2006). "Formulation of capillary hysteresis with internal state variables." *Water Resour. Res.*, 42(7), W07405.1–W07405.16.
Wheeler, S. J., Sharma, R. S., and Buisson, M. S. R. (2003). "Coupling of hydraulic hysteresis and stress-strain behaviour in unsaturated soils." *Géotechnique*, 53(1), 41–54.
Wheeler, S. J., and Sivakumar, V. (1995). "An elasto-plastic critical state framework for unsaturated soil." *Géotechnique*, 45(1), 35–53.
Yoshimine, M., Robertson, P. K., and Wride, C. E. (1999). "Undrained shear strength of clean sands to trigger flow liquefaction." *Can. Geotech.*, 36(5), 891–906.